JOURNAL OF THERMOPHYSICS AND HEAT TRANSFER
Vol. 24, No. 2, April–June 2010

Chemical Species and Nonequilibrium Temperatures for Airflows in a Plasma Wind Tunnel

F. De Filippis* and C. Purpura†
Centro Italiano Ricerche Aerospaziali, 81043 Capua, Italy
and
A. Viviani,‡ L. Acampora,§ and M. Fusco§
Seconda Università di Napoli, 81031 Aversa, Italy

DOI: 10.2514/1.43050

The flowfield generated by the plasma wind tunnel SCIROCCO is investigated by using optical emission spectroscopy, a diagnostic nonintrusive technique that is able to identify and analyze the chemical species in the flow. The physicochemical flow conditions are characterized by nonequilibrium effects that can result in large differences between rotational–translational, vibrational, and electronic temperatures. Thus, to study the freestream emission, the radiation emitted from a well-defined core volume on the plasma centerline during a test is collected by an optical system and analyzed by a spectrograph. Emission spectra are obtained over a 200–900 nm wavelength range. The experimental results are compared with the simulated spectra obtained by using the PARADE code to evaluate temperatures and concentrations of the air plasma species. Partial agreement is achieved between experimental and numerical data.

Nomenclature

c	=	speed of light
D_a	=	Damköhler number
H	=	enthalpy
I	=	current intensity
k	=	Boltzmann constant
M	=	Mach number
$\dot{M}$	=	mass flow rate
m	=	mass of the atom
n	=	number density
P	=	pressure
r	=	distance, parameter of Debye
T	=	temperature
t	=	time
V	=	voltage
w	=	half-width at half-maximum due to the interaction with the electrons
X	=	concentration
α	=	parameter that depends on the broadening due to the ions
$\Delta\lambda_D$	=	Doppler broadening
$\Delta\lambda_N$	=	natural broadening
$\Delta\lambda_P$	=	pressure (Stark) broadening
λ	=	wavelength
λ_{ul}	=	wavelength at the analyzed transition
ν	=	frequency
ρ	=	flow density

Subscripts

exit	=	exit nozzle section
o	=	total
p	=	permanence
r	=	relaxation
s	=	static
v	=	vibrational

Received 12 February 2009; revision received 15 October 2009; accepted for publication 25 October 2009.

*Head of Research Group, Space Laboratories; f.defilippis@cira.it.
†Researcher, Space Laboratories; c.purpura@cira.it.
‡Professor, Department of Aerospace and Mechanical Engineering; antonio.viviani@unina2.it. Senior Member AIAA.
§Graduate Student, Department of Aerospace and Mechanical Engineering.

I. Introduction

ONE of the most interesting and challenging research fields at the Centro Italiano Ricerche Aerospaziali (CIRA) is the simulation of atmospheric reentry conditions to test materials used for spacecraft thermal protection systems (TPS). The hypersonic flow encountered by a space vehicle is simulated using the plasma wind tunnel SCIROCCO located at the CIRA site.

The airflow encountered by an orbiter or capsule during atmospheric reentry as well as the plasma wind-tunnel simulated flow are characterized by thermal and chemical nonequilibrium effects because of the high velocity with respect to the typical low relaxation times of molecules. To determine the real thermodynamic and chemical state of these flows, the freestream can be analyzed with nonintrusive spectroscopy methodologies.

Optical emission spectroscopy represents a well-known nonintrusive diagnostic technique that has great potential for the determination of flow properties such as the rotational and vibrational temperatures of molecules, the electronic temperature of atoms, and the concentrations of all species composing the plasma airflow. Over the last few years, measurements by emission spectroscopy on air processes in arc-jet plasma wind tunnels have been extensively carried out to obtain information and data of interest [1–5].

In the CIRA Space Laboratories, the light emitted by the plasma jet during a SCIROCCO wind-tunnel test is investigated using a spectrometric data acquisition system. In this paper some experimental spectra obtained from a series of acquisitions during a test campaign are discussed. The primary goal of this work is to employ high-resolution spectroscopy [6] to identify the chemical composition and temperature (vibrational in particular) of the species present in the hypersonic flow. For this purpose, the experimental spectra have been corrected by a proper efficiency curve and compared with numerical predictions.

The radiation from all molecules present in the air plasma has been numerically estimated using the plasma radiation database PARADE [7,8] developed in the framework of an ESA/ESTEC (European

Space Research and Technology Centre) technical research project and made available to CIRA directly by ESA.

A valid estimation of the rotation–translation temperature of the flow jet is carried out by analyzing the molecular band emission shape of the nitrogen oxide in the 200–320 nm UV-light range. This band system has been clearly observed at the total enthalpy conditions of the SCIROCCO facility.

Another goal of this paper is to highlight that an atomic peak has also been observed due to the presence of O^+ atoms, whose emission is also possible at a not-very-high electronic temperature. A method that allows for the computation of the exit nozzle electronic density, starting from the peak broadening analysis, will be presented.

II. Theoretical Framework

A. Code PARADE

The plasma radiation database PARADE version 2.2 [7] code has been developed in the framework of an ESA/ESTEC technical research project. It can been used to calculate the radiation from all important molecules in air plasma radiation. For the atomic line radiation, the shape of the lines is assumed to have a Voigt profile.

PARADE is used for calculating the emission of electronically excited atoms and diatomic molecules both for radiation transport computations and for synthetic spectra generation, which can be used for comparison with the experimental ones. In Table 1 [7,8] we report the molecular electronic state levels considered in the PARADE code that are relevant to the species present in the air.

B. Vibrational and Chemical Nonequilibrium

When there are conditions in the flow for which the chemical and dissociation reactions become important and the hypersonic regimes are reached, the necessary time t_r for these phenomena to reach the equilibrium has to be taken into account [9]. If the residence time t_p of the fluid particles in a certain zone of the field is lower than t_r because of high values of flow speed, the expected conditions of chemical equilibrium, as represented by the local values of pressure and temperature, are not reached.

The parameter that governs such phenomenology is the Damköhler number given by

$$D_a = \frac{t_p}{t_r} \tag{1}$$

where D_a tends to zero, the chemical and vibrational properties of the fluid are substantially unchanged, and the flow is *frozen*. The case of *vibrational frozen flow* is representative of conditions for which the vibrational energy remains constant throughout the flow. For our experimental analysis this hypothesis is considered valid. Indeed, the high velocity of the molecules and atoms hinders relaxation of the vibrational energy during the expansion through the nozzle, so the vibrationally excited molecules keep the energetic level's distribution frozen.

To simulate the gas in chemical and vibrational nonequilibrium, CIRA has developed a computational code called H2NS (hypersonic two-dimensional Navier—Stokes) [10,11]. It can solve the full Navier–Stokes equations; the gas is modeled as a mixture of five reacting species O, N, NO, O_2, and N_2 (Park's model [9]), and those ionized are not considered because of their low concentration.

The nonequilibrium vibrational model implemented in this code is the one proposed by Millikan and White [12]. The H2NS code assumes that the electronic temperature is equal to the translational and rotational ones. This hypothesis consists of setting to zero the electronic relaxation time of all species present in the flow, which is considerably lower than the flow time across the nozzle.

The H2NS numerical calculation of the SCIROCCO exit hypersonic jet characteristics has been carried out by simulation of the flowfield into the whole convergent–divergent conical nozzle. To compare the experimental results with the numerical data, the latter are chosen at the center of the nozzle exit section and have been computed as described hereafter.

Input conditions at the convergent nozzle entrance have been supplied to the code based on total enthalpy and total pressure measured during the test, whereas other inlet quantities were obtained assuming equilibrium conditions of the air process; these inlet conditions are considered constant at the inlet surface of the convergent.

Essentially, the total pressure and total enthalpy at the exit of the constrictor are considered to have flat profiles. This aspect has been confirmed in the design phase of the SCIROCCO arc heater: the ratio between length and diameter of the constrictor is about 50 and this value is sufficiently high to guarantee that the enthalpy profile at the arc-heater exit is flat and not peaked at the centerline, as happens for low L/D ratios.

This thermo-fluid-dynamic analysis was conducted during the SCIROCCO design using the ARCFLO code, the same one used in a recent publication [13].

The temperature at the wall is assumed to be 300 K due to the fact that the nozzle walls are cooled by demineralized water recirculation. The accuracy of the computation is guaranteed by CIRA numerical group experience in the field of internal hypersonic flows simulation using the H2NS code. Computations carried out by the CIRA numerical department always abide by the criteria of grid independency. More computations are carried out in general with different grid thicknesses to be sure of this independency and the reader can refer to [10,11,14–16] for detailed justification. In addition, this set of

Table 1 Molecular transition implemented in PARADE version 2.2

Molecule	Name	Transition	PARADE	Under investigation
N_2	First positive	$B^3\Pi \rightarrow A^3\Sigma$	$^1\Pi \rightarrow {}^1\Sigma$ (zero)	$^1\Pi \rightarrow {}^1\Sigma$
N_2	Second positive	$C^3\Pi \rightarrow B^3\Pi$	$^1\Sigma \rightarrow {}^1\Sigma$ (zero)	$^3\Pi \rightarrow {}^3\Pi$
N_2	Birge–Hopfield	$B^1\Pi \rightarrow X^1\Sigma$	$^1\Pi \rightarrow {}^1\Sigma$ (one)	$^1\Pi \rightarrow {}^1\Sigma$
N_2^+	First negative	$B^2\Sigma \rightarrow X^2\Sigma$	$^1\Sigma \rightarrow {}^1\Sigma$ (zero)	$^2\Sigma \rightarrow {}^2\Sigma$
N_2^+	Meinel	$A^2\Pi \rightarrow X^2\Sigma$	$^2\Pi \rightarrow {}^2\Sigma$ (S2P2)	$^2\Pi \rightarrow {}^2\Sigma$
O_2	Schumann–Runge	$B^3\Sigma \rightarrow X^3\Sigma$	$^1\Sigma \rightarrow {}^1\Sigma$ (zero)	$^1\Sigma \rightarrow {}^1\Sigma$
NO	β	$B^2\Pi \rightarrow X^2\Pi$	$^1\Sigma \rightarrow {}^1\Sigma$ (zero)	$^2\Pi \rightarrow {}^2\Pi$
NO	γ	$A^2\Sigma \rightarrow X^2\Pi$	$^2\Sigma \rightarrow {}^2\Pi$ (S2P2)	$^2\Sigma \rightarrow {}^2\Pi$
NO	δ	$C^2\Pi \rightarrow X^2\Pi$	$^1\Sigma \rightarrow {}^1\Sigma$ (zero)	$^2\Pi \rightarrow {}^2\Pi$
NO	ε	$D^2\Sigma \rightarrow X^2\Pi$	$^2\Sigma \rightarrow {}^2\Pi$ (S2P2)	$^2\Sigma \rightarrow {}^2\Pi$
CN	Red	$A^2\Pi \rightarrow X^2\Sigma$	$^2\Pi \rightarrow {}^2\Sigma$ (S2P2)	$^2\Pi \rightarrow {}^2\Sigma$
CN	Violet	$B^2\Sigma \rightarrow X^2\Sigma$	$^1\Sigma \rightarrow {}^1\Sigma$ (zero)	$^2\Sigma \rightarrow {}^2\Sigma$
CO	Third positive	$A^3\Pi \rightarrow b^3\Pi$	$^1\Sigma \rightarrow {}^1\Sigma$ (zero)	$^3\Pi \rightarrow {}^3\Pi$
CO	Fourth positive	$X^1\Sigma \rightarrow A^1\Pi$	$^1\Sigma \rightarrow {}^1\Pi$ (one)	$^1\Sigma \rightarrow {}^1\Pi$
CO	Angström	$B^1\Sigma \rightarrow A^1\Pi$	$^1\Sigma \rightarrow {}^1\Pi$ (one)	$^1\Sigma \rightarrow {}^1\Pi$
CO^+	First negative	$B^2\Sigma \rightarrow X^2\Sigma$	$^1\Sigma \rightarrow {}^1\Sigma$ (zero)	$^2\Sigma \rightarrow {}^2\Sigma$
CH	3900 A	$B^2\Sigma \rightarrow X^2\Pi$	$^2\Sigma \rightarrow {}^2\Pi$ (S2P2)	$^2\Sigma \rightarrow {}^2\Pi$
CH	4300°	$A^2\Delta \rightarrow X^2\Pi$	$^1\Pi \rightarrow {}^1\Pi$ (zero)	$^2\Sigma \rightarrow {}^2\Pi$
C_2	Swan	$A^3\Pi \rightarrow d^3\Pi$	$^1\Sigma \rightarrow {}^1\Sigma$ (zero)	$^3\Pi \rightarrow {}^3\Pi$
NH	3360°	$X^3\Sigma \rightarrow A^3\Pi$	$^1\Sigma \rightarrow {}^1\Pi$ (one)	$^2\Sigma \rightarrow {}^2\Pi$

references shows that the thermochemical model used is suitable to calculate the expanding flowfield.

Analyzing the results obtained using the H2NS code, it is possible to note that the vibrational temperature of the N_2 molecule is higher than the O_2 and NO molecules. This phenomenon is due to the model of vibrational nonequilibrium of Millikan–White used in H2NS. From computational fluid dynamics (CFD) simulations of H2NS, the values of the thermodynamic parameters can be extracted, including the vibrational temperatures of the molecular species for various sections of the nozzle, corresponding to the exit sections of the various configurations of the SCIROCCO nozzle.

III. Experimental Setup

A. SCIROCCO Facility

The hypersonic jet analyzed by emission spectroscopy is generated by a large-scale arc-jet plasma wind-tunnel facility, which is called SCIROCCO and is located at CIRA in Capua, Italy.

The SCIROCCO schematic in Fig. 1 can be used to follow the process inside the facility. The compressed air mixture (16.7 bar of maximum pressure) is energized and transformed into plasma by a 5.5 m arc-heater (70 MW of maximum electric power) and sent through the plenum chamber in a convergent–divergent nozzle (3.5 kg/s of maximum mass flow rate). The latter component can be used in four different configurations: each one is characterized by a different exit-section diameter (900, 1150, 1350, and 1950 mm), whereas the throat section is the same for all (75 mm diameter). In the nozzle, the plasma expands and accelerates until it becomes a hypersonic flow that generates a shock wave on the model in the test chamber.

The freestream zone, upstream of the shock wave, is now the object of the spectrometric analysis. The flux exiting from the test chamber is reduced by a 50-m-long diffuser and cooled by a heat exchanger. After the heat exchanger, there is the vacuum system and the component called DeNOx that reduces the NO concentration in the exiting gaseous mixture. Each SCIROCCO stage component, from the arc heater to the heat exchanger, is equipped with its own water cooling system at the specific pressure corresponding to the thermal flux that must be disposed of.

B. Optical System

Figure 2 shows the spectrometric acquisition system structure available in the Space Laboratories at CIRA. It consists of several instruments. The first one is a UV-Nikkor objective (105 mm focal length and $f4.5$ maximum diaphragm aperture) that is mounted in an instrument box near one of the lateral windows of the SCIROCCO facility test chamber. It is focused on a finite volume in the freestream region near the centerline at a distance of 17 cm from the exit section of the nozzle. The volume characteristics can be derived from the

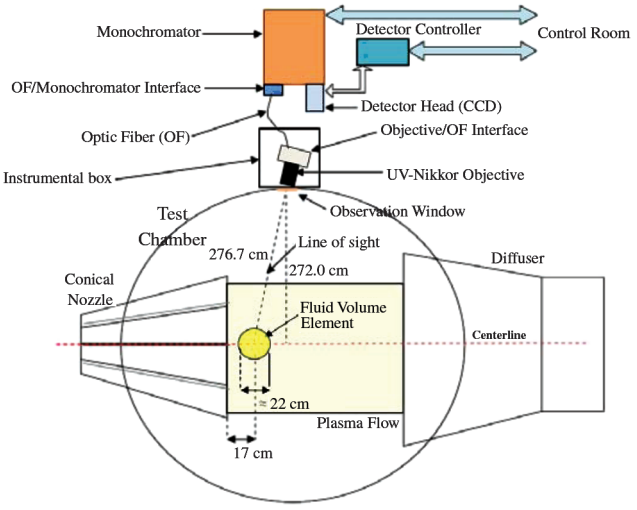

Fig. 2 Optical measurement scheme (elements are not in scale).

depth-of-field tables given in the UV-Nikkor instruction manual. Using the maximum diaphragm aperture of $f4.5$ at the distance of 3 m, the manual indicates a depth of field of about 11 cm behind and 11 cm in front of the focused point (on the line of sight). These data were confirmed by experimental tests performed moving a mercury lamp in each direction starting from the focused point; a significant intensity decay of the spectrum was found for distances greater than one depth of field, so a fluid element can be reasonably represented by a sphere with a diameter of 22 cm.

The radiation captured by the objective is sent by an optic fiber to the Jobin Yvon HR-460 monochromator entrance slit. In the monochromator, the radiation beam can be decomposed into its monochromatic components by a 1200 groove/mm holographic blazed grating. Behind the monochromator, there is a multichannel charge-coupled-device camera of 1024×256 pixels (pixel size: 26 μm) that is controlled by an appropriate controller. The whole spectrometer system is designed to work at a wavelength ranging from 200 to 900 nm. Monochromator and detection system data are acquired by using the software SynerJY installed on a PC situated in the SCIROCCO facility control room.

IV. Experimental Data

In April 2008, during a SCIROCCO test for a TPS system validation, seven spectroscopic acquisitions of freestream were carried out, all of them with the diffraction grating of 1200 groove/mm. The total enthalpy and total pressure reservoir conditions were essentially constant during the various acquisitions,

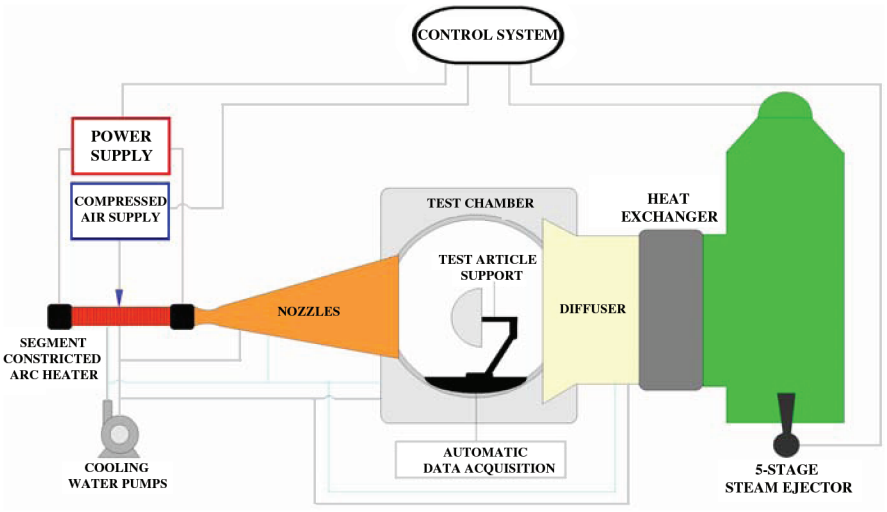

Fig. 1 Schematic of the SCIROCCO plasma wind tunnel.

which were obtained with 1) free-jet conditions and 2) a test model inserted into the jet.

Table 2 reports the quantities describing test conditions of runs by using the facility nozzle configuration of 1150 mm exit diameter, and Table 3 gives the corresponding numerical predictions. The spectrometer setup parameters used for each spectrometric acquisition during the experimental runs are reported in Table 4.

A. Measured Spectra

For each acquisition, an emission spectrum was plotted on a Cartesian diagram, the x axis of which represents wavelength values measured in nanometers and the y axis of which represents the relative radiative intensity measured in an arbitrary unit (counts). In Figs. 3–9, the seven spectra in their whole wavelength ranges are presented, and the total acquired spectra, obtained from the previous ones, are reported in Fig. 10. In the next paragraph, we will focus on and analyze some restricted and significant ranges.

B. Acquisition System Efficiency and Measured Spectra Correction

The acquired spectra are related to the luminous intensity received by the spectrometer and not to the actual light intensity emitted, so the efficiency of the measurement chain must be accounted for. The efficiency curve was obtained experimentally: a combined deuterium–tungsten lamp was used to cover part of the ultraviolet/visible/near-infrared range (i.e., the range of interest: 200–900 nm).

The percentage efficiency $\eta_{\%}$ was determined for each sample by dividing the experimental spectrum $S_{\exp}(\lambda)$ by the manufacturer's certified spectrum $S_{\text{ref}}(\lambda)$ and then multiplying the obtained value by 100:

$$\eta_{\%} = \frac{S_{\exp}(\lambda)}{S_{\text{ref}}(\lambda)} \cdot 100 \tag{2}$$

The above relation accounts for the effect of the whole measurement chain, in steady condition, excluding the quartz glass window influence; however, the material treatment and the manufacturer transmission curve allow excluding any relevant distortion effect. Figure 11 shows the comparison between the reference and the experimental emission lamp spectrum.

The associated percentage efficiency curve is shown in Fig. 12. The curve gives evidence of low efficiency below a wavelength of 220 nm (less than 10%), and so the quality of data interpretation in that region must be considered with care. Using the efficiency curve, it is possible to calculate a correction coefficient curve, which is reported in Fig. 13; it is obtained as the reciprocal of the efficiency and then normalized (to one). In Fig. 14 we report the total acquired spectrum, given in Fig. 10, corrected through the correction curve.

Table 2 Test conditions

Parameters	Values
P_o, bar	2.9 ± 0.1
P_{exit}, mbar	0.388 ± 0.001
P_s, mbar	13.4 ± 1.1
H_o, MJ/kg	11.6 ± 0.8
$\dot{M}_o$. kg/s	0.495 ± 0.005
V, V	6780 ± 200
I, A	1720 ± 30
Power, MW	11.66 ± 0.81

Table 3 CFD predictions

Parameters	Values
M_{exit}	7.8
ρ, kg/m^3	1.0101×10^{-4}
X_{O}	2.3291×10^{-1}
X_{N}	3.0271×10^{-2}
X_{NO}	2.0180×10^{-5}
X_{N_2}	7.3672×10^{-1}
X_{O_2}	7.7595×10^{-5}
T_s, K	498.73
T_o, K	7424
$T_v\text{N}_2$, K	2225
$T_v\text{NO}$, K	855
$T_v\text{O}_2$, K	861

V. Comparison Between Experiment and Numerical Prediction

To identify the molecular composition of the plasma flow, a comparison of low-resolution measurements was made using results from PARADE, which were based on the computational results obtained with the H2NS code (see Table 3). The experimental spectra interpretation is further complicated due to the overlapping of the spectra of the various molecular species, such as NO, N_2, and N_2^+.

Moreover, there should be the contribution of the atomic species that was ignored in the present analysis, because atom emission was not observed, except in one case, which will be discussed later. It is worth pointing out that the electronic temperature of atoms was assumed equal to the flow static temperature by considering the electronic energy relaxation time to be lower than the flow residence time in the nozzle.

Among molecular species, only NO was clearly observed through the γ transition between the A and the X electronic states and through the δ transition between the C and the X electronic states in the UV region.

The emission of the NO species represents the most promising spectral region for extracting information on flow temperature conditions. In Fig. 15, the spectral acquisition of the ultraviolet region of the 1200 groove/mm diffraction grating is reported and it clearly shows a series of bands due to the γ and δ emission of NO. Each band is due to a specific vibrational jump, and the shape of the band is related to the molecule distribution between the various rotational levels.

In the actual acquisition, a low spectrometer efficiency is present below the wavelength of 220 nm and a quantitative comparison between experimental data and PARADE numerical data is very difficult. At this stage, only a qualitative analysis and interpretation can be given.

A spectra comparison between numerical predictions and experimental results must be limited to the 220–340 nm range. The NO vibrational temperature reported in Table 3 was used for PARADE simulation. Partial agreement between simulated and experimental data can be observed in Fig. 15.

Table 4 Spectrometer setup parameters

Acquisition no.	PWT running no. 252	Entrance slit, mm	Exit slit, mm	Exposition time, s	Gain (x)	Grating, lines/mm	Wavelength range, nm
1	Free jet	0.5	2.1	1	4	1200	200–300
2	Free jet	0.5	2.1	1	4	1200	300–400
3	Free jet	0.5	2.1	1	4	1200	400–500
4	Free jet	0.5	2.1	1	4	1200	500–600
5	Free jet	0.5	2.1	1	4	1200	600–700
6	Free jet	0.5	2.1	1	4	1200	700–800
7	Model	0.5	2.1	1	4	1200	800–900

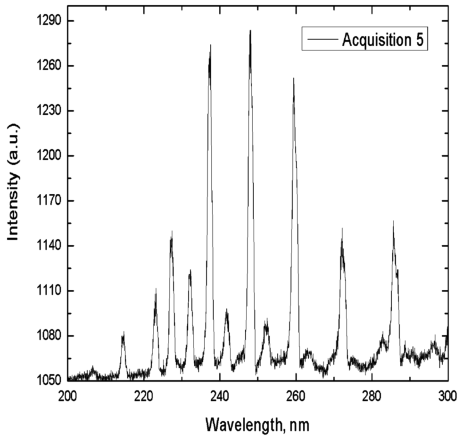

Fig. 3 Spectrum 1: free jet, 200–300 nm.

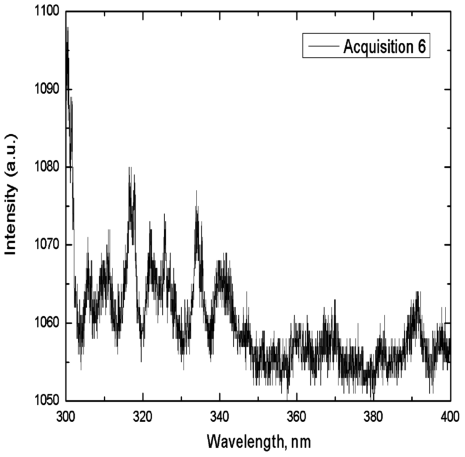

Fig. 4 Spectrum 2: free jet, 300–400 nm.

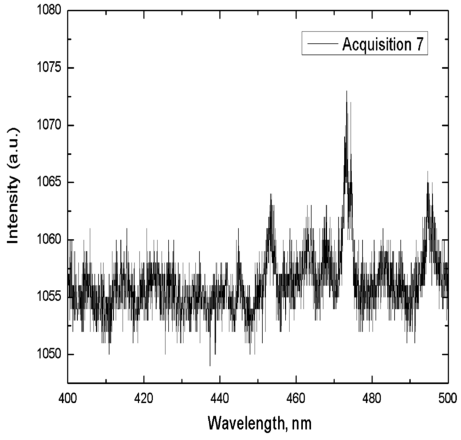

Fig. 5 Spectrum 3: free jet, 400–500 nm.

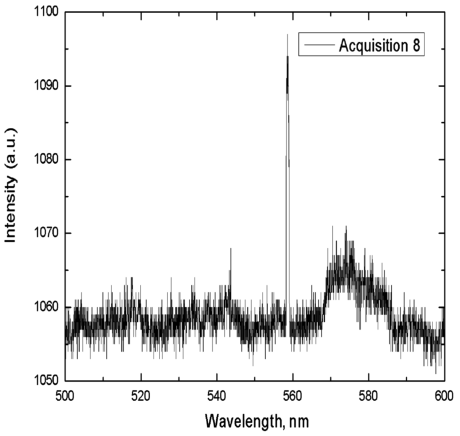

Fig. 6 Spectrum 4: free jet, 500–600 nm.

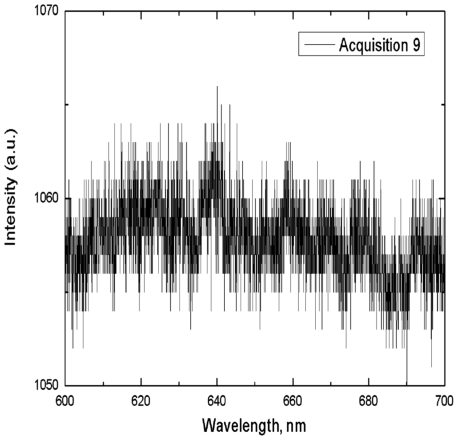

Fig. 7 Spectrum 5: free jet, 600–700 nm.

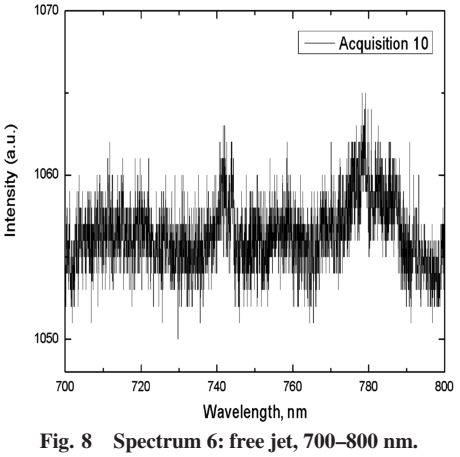

Fig. 8 Spectrum 6: free jet, 700–800 nm.

In particular, seven vibrational bands in the 225–300 nm range associated with the γ transition are very clear. Their wavelength position is consistent with the PARADE spectrum, but band shape and peak intensity are quite different, due to the numerical approximation of temperature and concentration. Moreover, there is no agreement between experimental and numerical data for the δ transition (C–X) vibrational bands, as for Fig. 16.

As mentioned before, the analysis of the NO emitted light can be used to obtain information on the flow temperature. In fact, the shape of each band is related to the NO rotational temperature and, in turn, the value of this temperature can be linked to the position of the maximum value registered for the specific band.

Therefore, under the hypothesis that the NO rotational temperature is linked to the flow static temperature, it is possible to define a deterministic method for the measurement of the flow static temperature of hypersonic jets in a plasma wind-tunnel facility.

The set of parameters that ensures the best consistency between measurement and calculation can be obtained in two steps. The first step is the normalization of the measured data so that the position of the vibrational band maximum, located around the 250 nm wavelength, does coincide (in general, this band is the best in terms of shape because of its location near the higher wavelength where the system efficiency has the lower criticality). The second step consists of the minimization of the ordinary least-squares function between

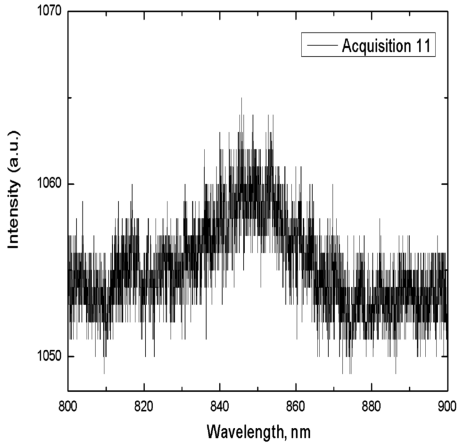

Fig. 9 Spectrum 7: free jet, 800–900 nm.

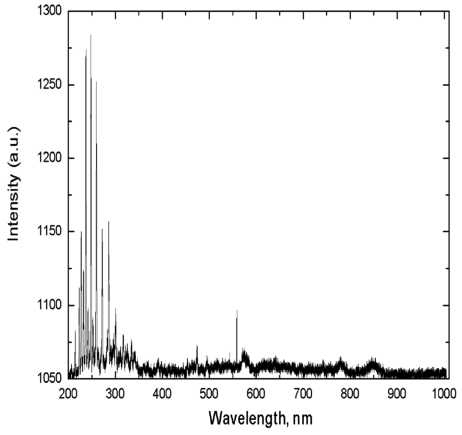

Fig. 10 Complete spectrum through diffraction grating of 1200 groves/mm.

experimental and theoretical data variation with respect the NO rotational temperature.

VI. Evaluation of Electronic Density Through Investigation of Ionized Oxygen Emission

By observing Fig. 8, we can note that an atomic peak is clearly visible at $\lambda = 558.621$ nm; this peak is also represented in Figs. 17 and 18. Actually, it is constantly observed in the SCIROCCO flow jet and it is the only spectral observation that can be attributed to an atomic emission. The peak is located in the visible region and it gives the flow the green coloring observed during the tests.

This peak is not predicted by PARADE computations, regardless of whatever change is applied to the simulation temperature. The atomic species, most likely to produce such a peak, are the atomic oxygen O and the positive ion of atomic oxygen O^+, even if we cannot exclude jet contamination by a metallic element. Further studies are in progress to clarify this point.

In any case, regardless of the origin of the atomic peak, it could be used to determine the electronic density of the plasma jet. An attempt in that direction was made and is hereafter described.

The shape of the spectral emission's atomic peak can give information about the electronic density and, specifically, the widening of the emission line must be analyzed. The widening of spectral line is due to several phenomena: 1) natural broadening, 2) pressure broadening, and 3) Doppler broadening.

1) The natural broadening $\Delta\lambda_N$ results in the present case are lower than the resolution of the instrument used. The instrumentation resolution is about 0.7 nm, and so the natural broadening is practically negligible.

2) The pressure broadening $\Delta\lambda_P$ is mainly due to the Stark broadening. This represents the interaction between transmitter and loaded particles, and it is mostly due to the electronic density and, to a lesser extent, to the electronic temperature. The pressure broadening can be obtained through the relation

$$\Delta\lambda_P = [1 + 1.75\alpha(1 - 0.75r)]w \tag{3}$$

where w is the half-width at half-maximum (HWHM) due to the interaction with the electrons, α is a parameter related to the broadening due to the ions, r is the parameter of Debye. To have an estimate of the maximum density at the end of the SCIROCCO nozzle, we observe that at the analyzed conditions ($p = 40$ Pa and $T = 435$ K), there is a number density in the gas of

$$n_{\text{air}} = \frac{p}{kT} = 6.7 \times 1021 \text{ part/m}^3$$

If we assume the degree of ionization at the beginning of the nozzle to be at its equilibrium value (of the order of 10^{-4}) and to be constant during the expansion, we can estimate the electronic density at the end of the nozzle in the order of 10^{17} to 10^{18} part/cm^3. For these values of electronic density, the pressure (Stark) broadening HWHM is very small:

$$8 \times 10^{-7} \leq \Delta\lambda_P \leq 8 \times 10^{-6} \tag{4}$$

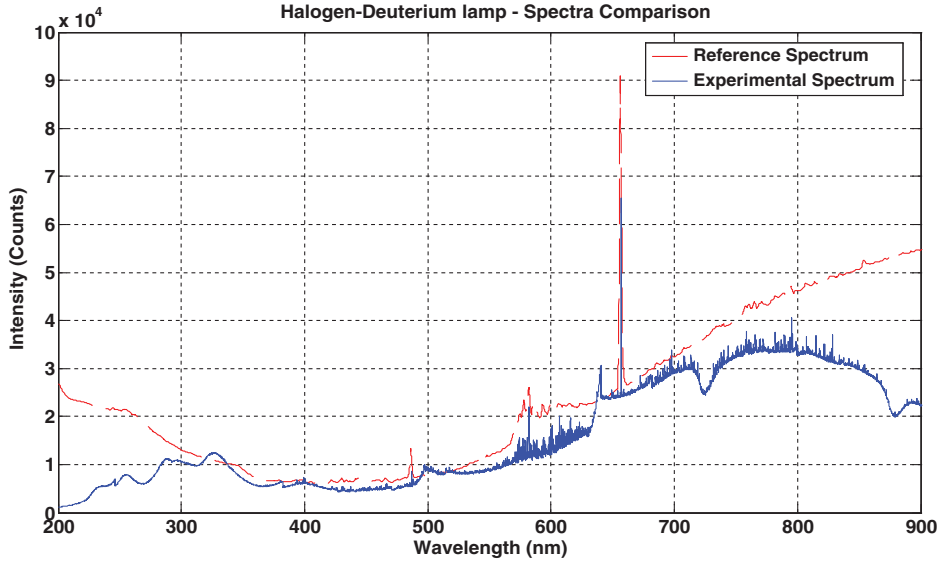

Fig. 11 Deuterium–tungsten lamp spectrum comparison.

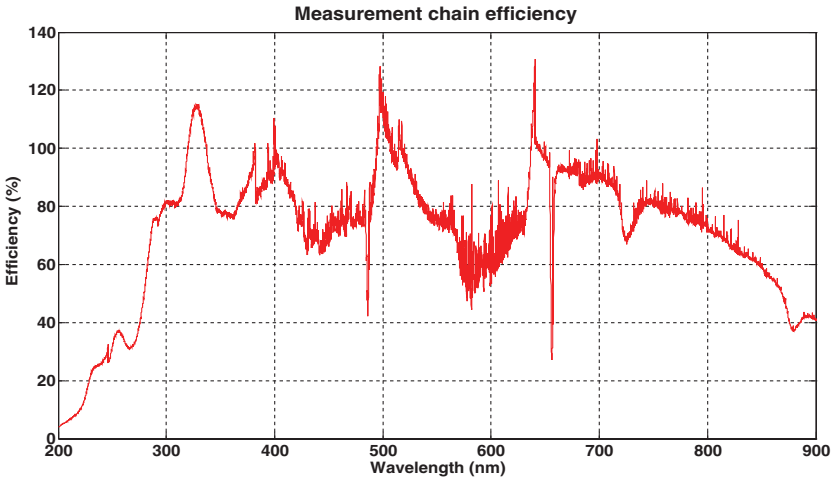

Fig. 12 Measurement chain percentage efficiency versus wavelength.

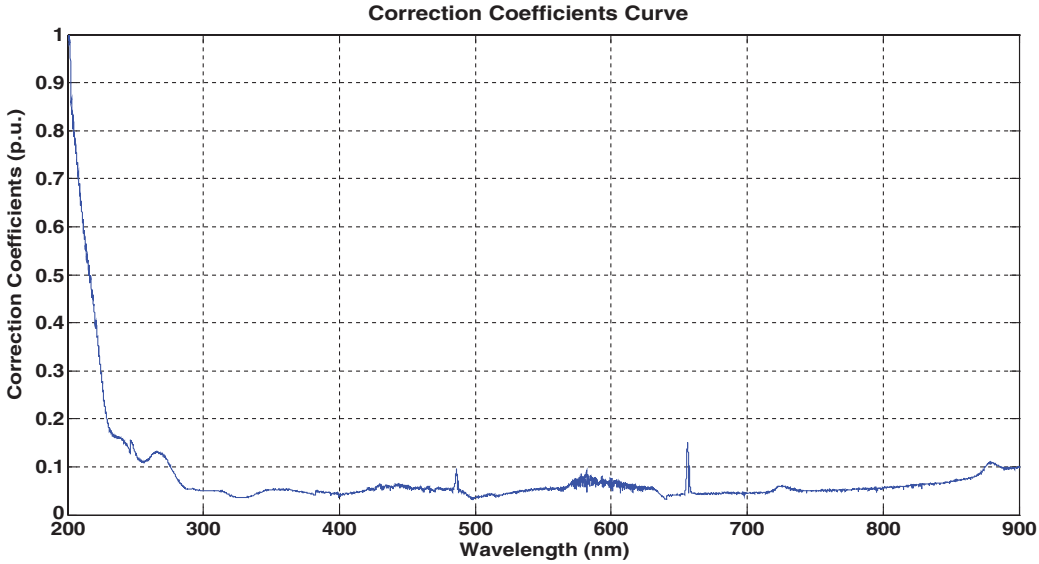

Fig. 13 Correction coefficient versus wavelength.

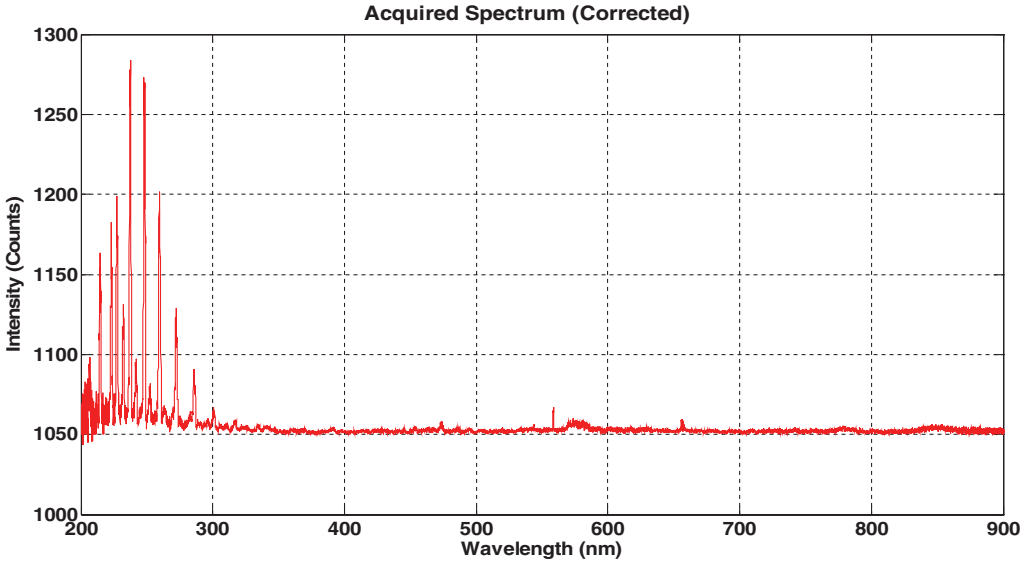

Fig. 14 Corrected acquired spectrum.

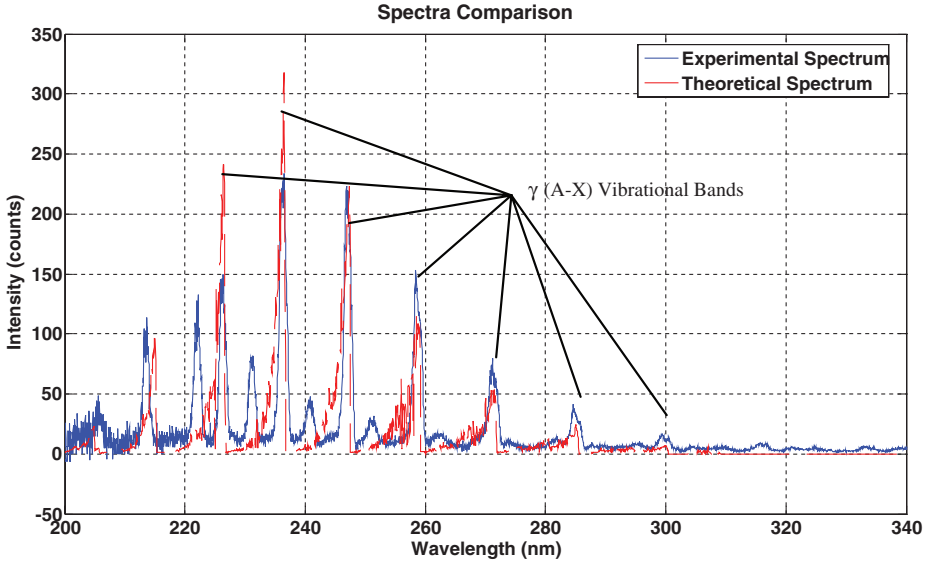

Fig. 15 Measured versus synthetic spectra in the range 200–340 nm.

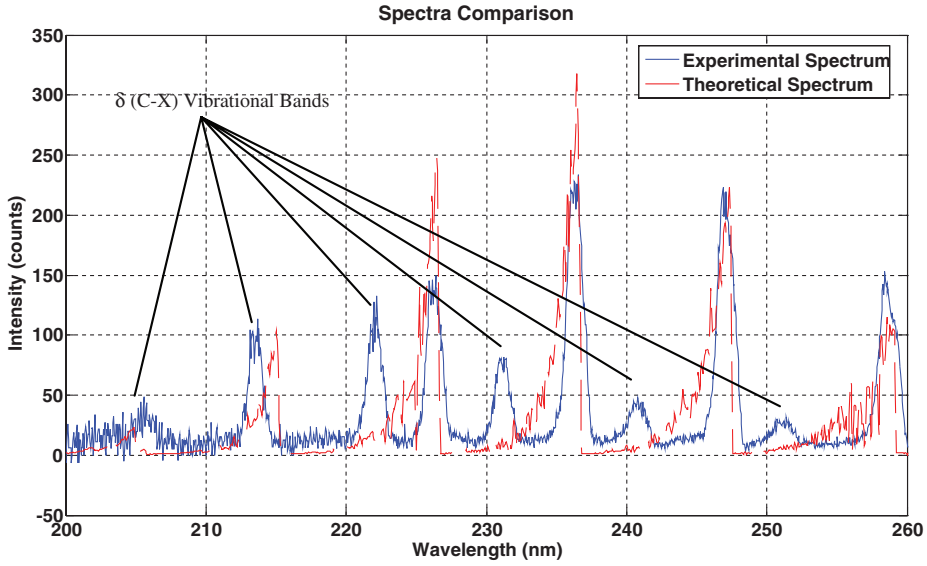

Fig. 16 The δ $(C–X)$ transition vibrational bands.

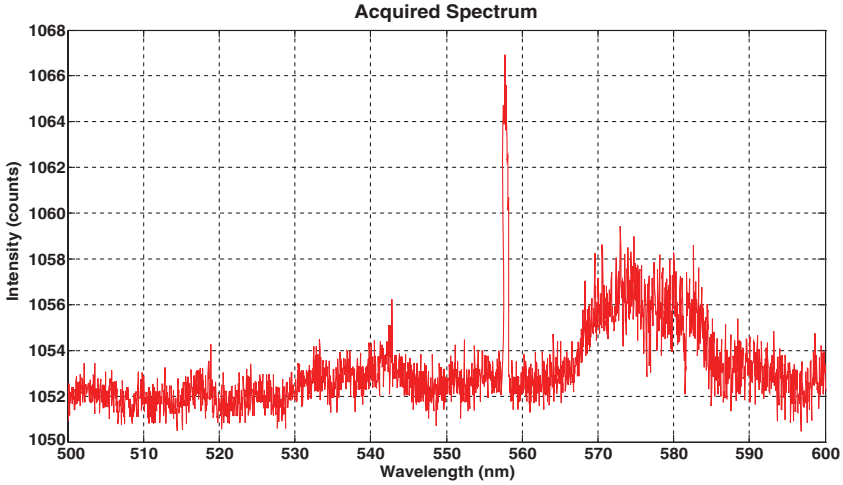

Fig. 17 Presence of an atomic peak.

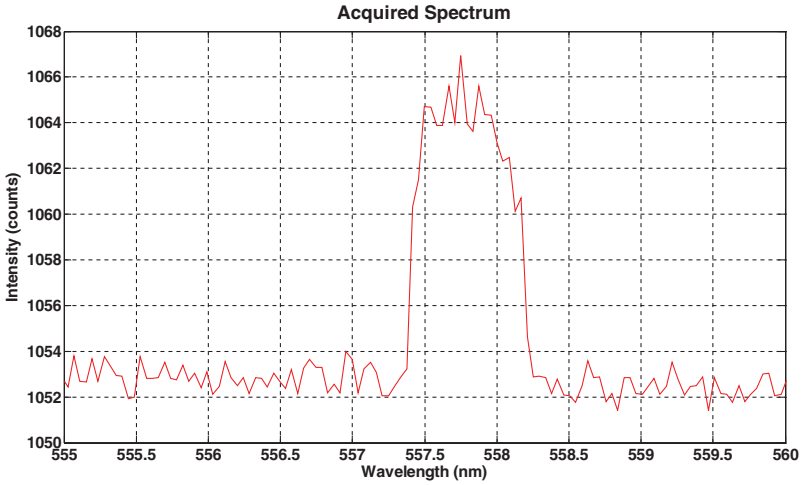

Fig. 18 Zoom on the previous peak.

3) The Doppler broadening depends on type and temperature of the transmitted element. The Doppler broadening HWHM is expressed as

$$\Delta\lambda_D = \lambda_{\text{ul}}\sqrt{\frac{2kT}{mc^2}} \tag{5}$$

where λ_{ul} is the wavelength at the analyzed transition and m is the mass of the atom.

If we consider a 435 K temperature at the end of the nozzle and a 600 nm transition of the ionized oxygen, the obtained HWHM Doppler broadening is

$$\Delta\lambda_D = 1.6 \times 10^{-3} \tag{6}$$

From the above elements, we can conclude the following:

1) The spectral line broadening is mainly due to the Doppler broadening.

2) Pressure (Stark) and Doppler broadenings, like the natural broadening, have smaller resolutions than the instruments resolution used in spectroscopy.

Unfortunately, we concluded that the previously exposed method cannot be used for the electronic density determination in plasma wind-tunnel flows, due to low-density conditions at the exit nozzle. Moreover, the selection of an entrance slit of 0.5 mm, to capture most of the radiation intensity, reduces the measurement chain resolution to about 0.7 nm, thus representing the most important contribution to the band broadening. Therefore, only the information on the peak position can be retrieved.

VII. Conclusions

In this paper, we have reported and discussed the results of a spectroscopic analysis of the light emitted by hypersonic jets. The study is relevant in the framework of noninvasive measurement tools in high-temperature flows as in the plasma wind tunnels.

In particular, we have considered flows established in a plasma wind-tunnel facility, called SCIROCCO and located at CIRA in Capua, Italy, during a test campaign in April 2008. An experimental spectroscopy system was realized, and a light spectrum in the wavelength range of 200–900 nm was recorded during the tests.

To date, spectroscopy represents the most suitable method to analyze a flow jet in terms of chemical and thermofluid-dynamic characteristics, since it is not possible to introduce any instrument into hypersonic flows. Nevertheless, the analysis of spectroscopic data is very complex due to the presence of various molecular and atomic species in chemical and thermal nonequilibrium, which makes it quite difficult to distinguish the superimposed effects; however, we have been able to identify the nitric oxide (A–X transition) vibrational bands.

The use of spectroscopy in SCIROCCO is very significant, because the flow jet has a diameter of up to 2 m, whereas the region focused on by the spectroscopy has a dimension of an order of magnitude less (10–20 cm). In this way, the light analyzed comes from a gas volume in which the thermofluid-dynamic parameters are essentially constant.

There is practically no risk that luminous signals might be contaminated by the light emitted by the boundary layer, characterized by very-high-temperature values and different chemical compositions. This risk must be considered when emission spectroscopy is carried out with low-power facilities.

The two main results of the present study are 1) the clear identification of nitric oxide presence through the γ transition and 2) the fact that the code PARADE does not correctly simulate the nitric oxide δ transition.

In addition, one atomic peak has been clearly observed at around 600 nm, the identification of which has not been possible. This peak is probably due to atomic oxygen or atomic oxygen's positive ion, but it can also be due to a metallic dust in the flow. This peak has been used to attempt a calculation of the flow electronic density by evaluation of the broadening size; the attempt was not successful because of the pressure and density conditions of the analyzed flow.

In the near future, we plan to establish the emission spectroscopy as a standard experimental data acquisition system at the SCIROCCO facility. In this way, we can implement continuous optimization of the experimental setup and can improve interpretation of results in our attempt to develop simple and accurate methods that link spectrum characteristics to flows quantities, the measure of which is of interest for the aerospace research.

Acknowledgments

We thank Salvatore Borrelli, Marco Marini, Antonio Schettino, and his coworkers for the use of the numerical code H2NS, developed at Centro Italiano Ricerche Aerospaziali (CIRA), and for their cooperation. We also thank ESA for making the code PARADE available to us.

References

[1] Rob, M. A., Mack, L. H., Jr., Arepalli, S., and Scott, C. D., "Characterization of Plenum Spectra in an Arcjet Wind Tunnel," *Journal of Thermophysics and Heat Transfer*, Vol. 11, No. 3, Oct.–Dec. 1997, pp. 339–345. doi:10.2514/2.6271

[2] Scott, C. D., Blackwell, H. E., Arepalli, S., and Akundi, M. A., "Techniques for Estimating Rotational and Vibrational Temperature in Nitrogen Arcjet Flows," *Journal of Thermophysics and Heat Transfer*, Vol. 12, No. 4, Oct.–Dec. 1998, pp. 457–464. doi:10.2514/2.6369

[3] Chung S. Park, Newfield, M. E., Fletcher, D. G., and Gőkçen, T., "Spectroscopic Measurements of Shock-Layer Flows in an Arcjet

Facility," *Journal of Thermophysics and Heat Transfer*, Vol. 13, No. 1, Jan.–March 1999, pp. 60–67.
doi:10.2514/2.6401

[4] Lago, V., Lebèhot, A., Dudeck, M., Pellerin, S., Renault, T., and Echegut, P., "Entry Conditions in Planetary Atmospheres: Emission Spectroscopy of Molecular Plasma Arcjets," *Journal of Thermophysics and Heat Transfer*, Vol. 15, No. 2, April–June 2001, pp. 168–175.
doi:10.2514/2.6605

[5] Matsuda, A., Fujita, K., Sato, S., and Abe, T., "Nonequilibrium Phenomena Behind Strong Shock Waves Generated in Superorbital Reentry Flight," *Journal of Thermophysics and Heat Transfer*, Vol. 18, No. 3, July–Sept. 2004, pp. 342–348.
doi:10.2514/1.6244

[6] Jacek Klinowski, *High Resolution Molecular Spectroscopy—Part 4: Electronic Spectroscopy*, Cambridge Univ., Dept. of Chemistry, Cambridge, England, U.K., 2003–2004.

[7] Smith, A. J., Wood, A., Dubois, J., Fertig, M., Pfeiffer, B., and Marraffa, L., "Plasma Radiation Database PARADE V2, Final Report Issue 2," ESA, Paris, July 2005.

[8] Winter, W., Pfeiffer B., Fertig M., and Auweter-Kurtz, M., "Extension of PARADE to CO_2 Plasmas and Comparison with Experimental Data in High Spectral Resolution for Air and CO_2 Species," *Proceedings of the 2nd International Workshop on Radiation of High Temperature Gases in Atmospheric Entry* [CD-ROM], SP-629, ESA, Noordwijk, The Netherlands, Nov. 2006.

[9] Anderson, J. D., *Hypersonic and High Temperature Gas Dynamics*, AIAA Education Series, AIAA, Reston, VA, 2006.

[10] Borrelli, S., and Schettino A., "Numerical Correlation Between Flight and Plasma Wind Tunnel Tests," *Journal of Spacecraft and Rockets*, Vol. 34, No. 3, 1997, pp. 397–399.

[11] De Filippis, F., and Borrelli, S., "Analysis of Different Approximation Levels Introduced in the Developments for Transport Coefficients Models of High Energy Air," *Proceedings of the 19th Congress of the International Council of the Aeronautical Sciences (ICAS-94)*, Vol. 1, International Council of the Aeronautical Sciences, Stockholm, Sept. 1994, pp. 398–405.

[12] Millikan, R. C., and White, D. R., "Systematic of Vibrational Relaxation," *Journal of Chemical Physics*, Vol. 39, No. 12, 1963, pp. 3209–3213.
doi:10.1063/1.1734182

[13] Sakai, T., Suzuki, T., Fujita, K, and Ito, T., "Calculation of High Enthalpy Environment in an Arcjet Facility," *Journal of Thermophysics and Heat Transfer*, Vol. 21, No. 1, 2007, pp. 249–251.
doi:10.2514/1.26963

[14] De Filippis, F., Del Vecchio, A., Marini, M., Borrelli, S., and Caristia, S. "CIRA 70-MW Plasma Wind Tunnel: A Comparison Between Measured and Computed Nozzle Flows Profiles," *Proceedings of the Euromech 440 Conference*, Institut Universitaire des Systèmes Thermiques Industriels, Marseilles, France, 16–19 Sept. 2002, pp. 51–53.

[15] Marini, M., and Graps, E., "Aerothermodynamic Analysis of a IRT-Capsule in Flight Conditions and Design/Execution of Plasma Wind Tunnel Tests," 13th AIAA International Space Planes and Hypersonic Systems and Technologies Conference, AIAA Paper 2005-3279, Capua, Italy, May 2005.

[16] De Filippis, F., Purpura, C., Viviani, A., Acampora, L., and Fusco, M., "Thermochemical Analysis of Plasma Wind Tunnel Air Flow by High resolution Spectroscopy," 47th AIAA Aerospace Sciences Meeting and Exhibit AIAA Paper 2009-1596, Orlando FL, 5–8 Jan. 2009.